Energy-momentum time integration of gradient-based models for fiber-bending stiffness in anisotropic thermo-viscoelastic continua

J. Dietzsch[1], M. Groß[2] and I. Kalaimani[3]

[1] Technische Universität Chemnitz, Professorship of applied mechanics and dynamics Reichenhainer Straße 70, D-09126 Chemnitz, julian.dietzsch@mb.tu-chemnitz.de

[2] michael.gross@mb.tu-chemnitz.de [3] iniyan.kalaimani@mb.tu-chemnitz.de

Key words: Fiber-bending stiffness, fiber-reinforced materials, locking behavior, mixed finite elements, mixed variational principle, gradient elasticity.

Abstract: *For our research, we are motivated by dynamic simulations of 3D fiber-reinforced materials in lightweight structures. In such materials, the material reinforcement is performed by fiber rovings with a separate bending stiffness, which can be modelled by a second-order gradient of the deformation mapping (see Reference [1]). Therefore, we extend a thermo-viscoelastic Cauchy continuum for fiber-matrix composites with single fibers by an independent field for the gradient of the right Cauchy-Green tensor. On the other hand, we focus on numerically stable dynamic long-time simulations with locking free meshes, and thus use higher-order accurate energy-momentum schemes emanating from mixed finite element methods. Hence, we adapt the variational-based space-time finite element method in Reference [2] to the new material formulation, and additionally include independent fields to obtain well-known mixed finite elements [3, 4, 5]. As representative numerical example, Cook's cantilever beam is considered. We primarily analyze the influence of the fiber bending stiffness, as well as the spatial and time convergence up to cubic order. Furthermore, we look at the influence of the physical dissipation in the material.*

1 INTRODUCTION

We consider an anisotropic material with the fiber roving direction $\boldsymbol{a}_0$, moving in the Euclidean space $\mathbb{R}^{n_{\text{dim}}}$ with the constant ambient temperature Θ_∞. The strain energy function of the material with a thermo-viscoelastic matrix and a thermoelastic fiber roving is given by

$$\Psi(\boldsymbol{C},\boldsymbol{C}_v,\Theta,\boldsymbol{a}_0) = \Psi_{\text{M}}(\boldsymbol{C},\boldsymbol{C}_v,\Theta) + \Psi_{\text{F}}(\boldsymbol{C},\Theta,\boldsymbol{a}_0) + \Psi^{\text{X}}_{\text{HOG}}(\dots,\boldsymbol{a}_0), \tag{1}$$

which is split into a matrix part Ψ_{M} a fiber roving part Ψ_{F} and a higher-order gradient part $\Psi^{\text{X}}_{\text{HOG}}$. Here $\boldsymbol{F} = \nabla \boldsymbol{q}$ define the deformation gradient by the position $\boldsymbol{q}$, $\boldsymbol{C} = \boldsymbol{F}^T\boldsymbol{F}$ define the right Cauchy-Green tensor, $\boldsymbol{C}_v$ define the viscous right Cauchy-Green tensor and Θ define the absolute temperature. The specific dependencies are given by

$$\Psi_{\text{M}}(\boldsymbol{C},\boldsymbol{C}_v,J,\Theta) = \Psi^{\text{iso}}_{\text{M}}(\boldsymbol{C},J) + \Psi^{\text{vol}}_{\text{M}}(J) + \Psi^{\text{cap}}_{\text{M}}(\Theta) + \Psi^{\text{coup}}_{\text{M}}(\Theta,J) + \Psi^{\text{vis}}_{\text{M}}(\boldsymbol{C}\boldsymbol{C}_v^{-1}) \tag{2}$$

$$\Psi_{\text{F}}(\boldsymbol{C},\Theta,\boldsymbol{a}_0,\dots) = \Psi^{\text{ela}}_{\text{F}}(\boldsymbol{C},\boldsymbol{a}_0) + \Psi^{\text{cap}}_{\text{F}}(\Theta) + \Psi^{\text{coup}}_{\text{F}}(\Theta,\boldsymbol{C}) \tag{3}$$

with the volume dilatation $J(\boldsymbol{C}) = \det[\boldsymbol{F}] = \sqrt{\det[\boldsymbol{C}]}$. The elastic part of the matrix function Ψ_{M} is split into an isochoric part $\Psi^{\text{iso}}_{\text{M}}$, a volumetric part $\Psi^{\text{vol}}_{\text{M}}$, a heat capacity part $\Psi^{\text{cap}}_{\text{M}}$, a part of the thermo-mechanical coupling effect $\Psi^{\text{coup}}_{\text{M}}$ and the viscoelastic free energy function of the matrix $\Psi^{\text{vis}}_{\text{M}}$. The parts of the fiber free energy is separated in the same manner. It is split into an elastic part $\Psi^{\text{ela}}_{\text{F}}$, a heat capacity part $\Psi^{\text{cap}}_{\text{F}}$ and a part of the thermo-mechanical coupling effect $\Psi^{\text{coup}}_{\text{F}}$. The functions of the

https://doi.org/10.4995/YIC2021.2021.12358

thermo-mechanical coupling $\Psi_{\mathrm{X}}^{\mathrm{coup}}$ with the coefficients of linear thermal expansion β_{X}, the structural tensor $\boldsymbol{M} = \boldsymbol{a}_0 \otimes \boldsymbol{a}_0$ and the fourth invariant $I_4 = \mathrm{tr}[\boldsymbol{C}\boldsymbol{M}]$ are given by

$$\Psi_{\mathrm{M}}^{\mathrm{coup}} = -2n_{\mathrm{dim}}\beta_{\mathrm{M}}(\Theta - \Theta_\infty)J\frac{\partial \Psi_{\mathrm{M}}^{\mathrm{vol}}(J)}{\partial J} \quad \Psi_{\mathrm{F}}^{\mathrm{coup}} = -2\beta_{\mathrm{F}}(\Theta - \Theta_\infty)\sqrt{I_4}\frac{\partial \Psi_{\mathrm{F}}^{\mathrm{ela}}(I_4,\dots)}{\partial I_4} \tag{4}$$

We distinguish between two different variants for the higher-order gradient part $\Psi_{\mathrm{HOG}}^{\mathrm{X}}$. One concerning the gradient of the deformation gradient $\boldsymbol{F}$ and one concerning the gradient of the right Cauchy-Green tensor $\boldsymbol{C}$. In comparison with $\Psi_{\mathrm{F}}^{\mathrm{ela}}$ which considers the fiber roving stretch, this part capture the bending of the fiber roving. The formulation regarding $\boldsymbol{F}$ is shown in Reference [1]. Here the sixth and seventh invariants are given by

$$I_6^{\mathrm{F}}(\boldsymbol{F},\nabla\boldsymbol{F}) = \boldsymbol{\kappa}_0^{\mathrm{F}} \cdot \boldsymbol{\kappa}_0^{\mathrm{F}} \qquad I_7^{\mathrm{F}}(\boldsymbol{F},\nabla\boldsymbol{F},\boldsymbol{C}) = \boldsymbol{\kappa}_0^{\mathrm{F}} \cdot \boldsymbol{C} \cdot \boldsymbol{\kappa}_0^{\mathrm{F}} \qquad \boldsymbol{\kappa}_0^{\mathrm{F}} = \boldsymbol{\Lambda}^{\mathrm{F}} \cdot \boldsymbol{a}_0 \tag{5}$$

with the referential representation

$$\boldsymbol{\Lambda}^{\mathrm{F}}(\boldsymbol{F},\nabla\boldsymbol{F}) = \boldsymbol{F}^T \cdot \boldsymbol{a}_0 \cdot \nabla\boldsymbol{F}^T \tag{6}$$

It is important to note here, that I_7 is depend on $\boldsymbol{C}$ as well as $\boldsymbol{\Lambda}$. Thus, for the strain energy function of the higher-order gradient, the dependencies are

$$\Psi_{\mathrm{HOG}}^{\mathrm{F}}(\boldsymbol{\Lambda}^{\mathrm{F}},\boldsymbol{C},\boldsymbol{a}_0) \quad = \quad \hat{f}(I_6^{\mathrm{F}}(\boldsymbol{\Lambda}^{\mathrm{F}}), I_7^{\mathrm{F}}(\boldsymbol{\Lambda}^{\mathrm{F}},\boldsymbol{C})) \tag{7}$$

A variant of the higher-order gradient formulation in $\boldsymbol{C}$ is shown in Reference [6]. From this we derive the following formula for the sixth invariant

$$I_6^{C}(\nabla\boldsymbol{C}) = (\boldsymbol{a}_0 \cdot \nabla\boldsymbol{C} \cdot \boldsymbol{a}_0) \cdot (\boldsymbol{a}_0 \cdot \nabla\boldsymbol{C} \cdot \boldsymbol{a}_0) \tag{8}$$

If we now set

$$\boldsymbol{\Lambda}^{\mathrm{C}}(\nabla\boldsymbol{C}) = \boldsymbol{a}_0 \cdot \nabla\boldsymbol{C} \tag{9}$$

we get the same expressions for the invariants as for $\boldsymbol{F}$, given by

$$I_6^{\mathrm{C}}(\nabla\boldsymbol{C}) = \boldsymbol{\kappa}_0^{\mathrm{C}} \cdot \boldsymbol{\kappa}_0^{\mathrm{C}} \qquad I_7^{\mathrm{C}}(\boldsymbol{C},\nabla\boldsymbol{C}) = \boldsymbol{\kappa}_0^{\mathrm{C}} \cdot \boldsymbol{C} \cdot \boldsymbol{\kappa}_0^{\mathrm{C}} \qquad \boldsymbol{\kappa}_0^{\mathrm{C}} = \boldsymbol{\Lambda}^{\mathrm{C}} \cdot \boldsymbol{a}_0 \tag{10}$$

and the final dependencies read

$$\Psi_{\mathrm{HOG}}^{\mathrm{C}}(\nabla\boldsymbol{C},\boldsymbol{C},\boldsymbol{a}_0) = f(I_6^{\mathrm{C}}(\nabla\boldsymbol{C}), I_7^{\mathrm{C}}(\nabla\boldsymbol{C},\boldsymbol{C})) \tag{11}$$

2 FINITE ELEMENT FORMULATION

The finite element discretization follows from the mixed principle of virtual power (see Reference [5, 2]). Here, we need the complete internal energy, which consists of the assumed temperature field $\tilde{\Theta}$, the entropy density field η as the corresponding Lagrange multiplier, the superimposed stress tensor $\tilde{\boldsymbol{S}}$ to derive an energy–momentum scheme, an independent mixed field $\tilde{\boldsymbol{C}}$ and the corresponding Lagrange multiplier $\boldsymbol{S}$. The internal energy functional reads

$$\begin{aligned}\Pi^{\mathrm{int}} = &\int_{\mathcal{B}_0} \Psi_{\mathrm{M}}(\tilde{\boldsymbol{C}},\tilde{J},\Theta)\mathrm{d}V + \int_{\mathcal{B}_0} \Psi_{\mathrm{F}}(\tilde{\boldsymbol{C}}_A,\Theta)\mathrm{d}V + \int_{\mathcal{B}_0} \frac{1}{2}\boldsymbol{S} : (\boldsymbol{C}(\boldsymbol{q}) - \tilde{\boldsymbol{C}})\mathrm{d}V + \int_{\mathcal{B}_0} \tilde{\boldsymbol{S}} : \tilde{\boldsymbol{C}}\mathrm{d}V \\ &+ \int_{\mathcal{B}_0} \eta\,(\Theta - \tilde{\Theta}) + \int_{\mathcal{B}_0} p\,(J(\tilde{\boldsymbol{C}}) - \tilde{J})\mathrm{d}V + \int_{\mathcal{B}_0} \tilde{p}\tilde{J}\mathrm{d}V + \int_{\mathcal{B}_0} \frac{1}{2}\boldsymbol{S}_A : (\tilde{\boldsymbol{C}} - \tilde{\boldsymbol{C}}_A)\mathrm{d}V \\ &+ \int_{\mathcal{B}_0} \tilde{\boldsymbol{S}}_A : \tilde{\boldsymbol{C}}_A\mathrm{d}V + \Pi_{\mathrm{HOG}}^{\mathrm{X}}\end{aligned} \tag{12}$$

We introduce an independent volume dilatation $\tilde{J}$ (see Reference [3]) and the field $\tilde{\boldsymbol{C}}_A$ (see Reference [4]) for the anisotropic part Ψ_{F} to avoid locking effects. Here, the Lagrange multiplier p plays the role of the hydrostatic pressure and the Lagrange multiplier $\boldsymbol{S}_A$ represents the stress tensor of the anisotropic part. To obtain an energy–momentum scheme, we also introduce the superimposed pressure $\tilde{p}$ and superimposed stress tensor $\tilde{\boldsymbol{S}}_A$. For the higher-order gradient fomulation with respect to $\boldsymbol{F}$ (HF), we introduce an independent field for $\boldsymbol{F}$, for $\nabla\boldsymbol{F}$ and for $\boldsymbol{\Lambda}^{\mathrm{F}}$

$$\begin{aligned}\Pi^{\mathrm{F}}_{\mathrm{HOG}} = &\int_{\mathcal{B}_0} \tilde{\boldsymbol{P}} : (\boldsymbol{F} - \tilde{\boldsymbol{F}})\mathrm{d}V + \int_{\mathcal{B}_0} \boldsymbol{B} \odot_3 (\nabla(\tilde{\boldsymbol{F}}) - \tilde{\boldsymbol{\Gamma}})\mathrm{d}V + \int_{\mathcal{B}_0} \boldsymbol{H} : (\boldsymbol{\Lambda}^{\mathrm{F}}(\tilde{\boldsymbol{F}}, \tilde{\boldsymbol{\Gamma}}) - \tilde{\boldsymbol{\Lambda}})\mathrm{d}V \\ &+ \int_{\mathcal{B}_0} \Psi^{\mathrm{F}}_{\mathrm{HOG}}(\tilde{\boldsymbol{\Lambda}}, \tilde{\boldsymbol{C}}_A, \boldsymbol{a}_0)\mathrm{d}V + \int_{\mathcal{B}_0} \tilde{\boldsymbol{H}} : \tilde{\boldsymbol{\Lambda}}\mathrm{d}V \end{aligned} \tag{13}$$

By the independent definition of $\tilde{\boldsymbol{F}}$ and $\tilde{\boldsymbol{\Gamma}}$ it is later in the discrete setting not necessary to construct a double gradient of the spatial shape functions. The introduction of $\tilde{\boldsymbol{\Lambda}}$ is necessary to have an objective quantity for the construction of an energy–momentum scheme with the superimposed field $\tilde{\boldsymbol{H}}$. For the higher-order gradient fomulation with respect to $\boldsymbol{C}$ (HC), we build the functional in a similar way

$$\begin{aligned}\Pi^{\mathrm{C}}_{\mathrm{HOG}} = &\int_{\mathcal{B}_0} \frac{1}{2}\boldsymbol{S}_G : (\boldsymbol{C} - \tilde{\boldsymbol{C}}_G) + \int_{\mathcal{B}_0} \boldsymbol{B} \odot_3 (\nabla(\tilde{\boldsymbol{C}}_G) - \tilde{\boldsymbol{\Gamma}})\mathrm{d}V + \int_{\mathcal{B}_0} \Psi^{\mathrm{C}}_{\mathrm{HOG}}(\tilde{\boldsymbol{\Gamma}}, \tilde{\boldsymbol{C}}_A, \boldsymbol{a}_0)\mathrm{d}V \\ &+ \int_{\mathcal{B}_0} \tilde{\boldsymbol{B}} \odot_3 \tilde{\boldsymbol{\Gamma}}\mathrm{d}V \end{aligned} \tag{14}$$

We introduce an independent field for $\boldsymbol{C}$ and $\nabla\boldsymbol{C}$. The further field with respect to $\boldsymbol{C}$ is introduced because $\boldsymbol{S}_G$ is assumed to be asymmetric, and therefore no symmetries in the Voigt notation are used later in the programming. Compared to the formulation in $\boldsymbol{F}$ (HF), we build the superimposed field based on $\tilde{\boldsymbol{\Gamma}}$. Furthermore, this leads to a less complex weak form. The superimposed fields (see Reference [2] and [5]), which have both variants in common, are given by

$$\tilde{\boldsymbol{S}} = \frac{\tilde{\Psi}(1) - \tilde{\Psi}(0) - \int \frac{\partial \Psi^{\mathrm{iso}}_{\mathrm{M}}}{\partial \tilde{\boldsymbol{C}}} : \dot{\tilde{\boldsymbol{C}}} - \int \frac{\partial (\Psi^{\mathrm{cap}}_{\mathrm{M}} + \Psi^{\mathrm{cap}}_{\mathrm{F}})}{\partial \Theta}\dot{\Theta} - \int \frac{\partial \Psi^{\mathrm{vis}}_{\mathrm{M}}}{\partial \boldsymbol{C}_v} : \dot{\boldsymbol{C}}_v}{\dot{\tilde{\boldsymbol{C}}} : \dot{\tilde{\boldsymbol{C}}}}\dot{\tilde{\boldsymbol{C}}} \tag{15}$$

$$\tilde{p} = \frac{\tilde{\Psi}(1) - \tilde{\Psi}(0) - \int \frac{\partial (\Psi^{\mathrm{iso}}_{\mathrm{M}} + \Psi^{\mathrm{vol}}_{\mathrm{M}})}{\partial \tilde{J}}\dot{\tilde{J}} - \int \frac{\partial \Psi^{\mathrm{coup}}_{\mathrm{M}}}{\partial \Theta}\dot{\Theta}}{\dot{\tilde{J}}\dot{\tilde{J}}}\dot{\tilde{J}} \tag{16}$$

$$\tilde{\boldsymbol{S}}_A = \frac{\tilde{\Psi}(1) - \tilde{\Psi}(0) - \int \frac{\partial \Psi^{\mathrm{ela}}_{\mathrm{F}}}{\partial \tilde{\boldsymbol{C}}_A} : \dot{\tilde{\boldsymbol{C}}}_A - \int \frac{\partial \Psi^{\mathrm{coup}}_{\mathrm{F}}}{\partial \Theta}\dot{\Theta}}{\dot{\tilde{\boldsymbol{C}}}_A : \dot{\tilde{\boldsymbol{C}}}_A}\dot{\tilde{\boldsymbol{C}}}_A \tag{17}$$

and the superimposed fields regarding the different higher-order gradient formulations read

$$\tilde{\boldsymbol{H}} = \frac{\tilde{\Psi}(1) - \tilde{\Psi}(0) - \int \frac{\partial \Psi^{\mathrm{F}}_{\mathrm{HOG}}}{\partial \tilde{\boldsymbol{\Lambda}}} : \dot{\tilde{\boldsymbol{\Lambda}}}}{\dot{\tilde{\boldsymbol{\Lambda}}} : \dot{\tilde{\boldsymbol{\Lambda}}}}\dot{\tilde{\boldsymbol{\Lambda}}} \qquad \tilde{\boldsymbol{B}} = \frac{\tilde{\Psi}(1) - \tilde{\Psi}(0) - \int \frac{\partial \Psi^{\mathrm{C}}_{\mathrm{HOG}}}{\partial \tilde{\boldsymbol{\Gamma}}} \odot_3 \dot{\tilde{\boldsymbol{\Gamma}}}}{\dot{\tilde{\boldsymbol{\Gamma}}} \odot_3 \dot{\tilde{\boldsymbol{\Gamma}}}}\dot{\tilde{\boldsymbol{\Gamma}}} \tag{18}$$

For the mixed principle of virtual power, we also need the kinetic power, given by

$$\dot{T} = \int_{\mathcal{B}_0} (\rho_0 \boldsymbol{v} - \boldsymbol{p}) \cdot \dot{\boldsymbol{v}}\mathrm{d}V + \int_{\mathcal{B}_0} \dot{\boldsymbol{p}} \cdot (\dot{\boldsymbol{q}} - \boldsymbol{v})\mathrm{d}V + \int_{\mathcal{B}_0} \boldsymbol{p} \cdot \ddot{\boldsymbol{q}}\mathrm{d}V \tag{19}$$

with the velocity $\boldsymbol{v}$, the linear momentum $\boldsymbol{p}$ and the mass density ρ_0. As external power, we assume

$$\begin{aligned}\dot{\Pi}^{\mathrm{ext}} = &-\int_{\mathcal{B}_0} \rho_0 \boldsymbol{g} \cdot \dot{\boldsymbol{q}}\mathrm{d}V - \int_{\partial\mathcal{B}_0} \boldsymbol{\lambda}_q \cdot (\dot{\boldsymbol{q}} - \dot{\boldsymbol{q}}^{\mathrm{ref}})\mathrm{d}A + \int_{\mathcal{B}_0} \nabla\left(\frac{\tilde{\Theta}}{\Theta}\right) \cdot \boldsymbol{Q}\mathrm{d}V + \int_{\mathcal{B}_0} \frac{\tilde{\Theta}}{\Theta} D^{\mathrm{int}}\mathrm{d}V \\ &+ \int_{\mathcal{B}_0} \dot{\boldsymbol{C}}_v : \mathbb{V}(\boldsymbol{C}_v) : \dot{\boldsymbol{C}}_v\mathrm{d}V \quad \boldsymbol{Q} = -\left[J(\tilde{\boldsymbol{C}}_A)\frac{k_{\mathrm{F}} - k_{\mathrm{M}}}{\tilde{\boldsymbol{C}}_A : \boldsymbol{M}}\boldsymbol{M} + kJ(\tilde{\boldsymbol{C}})\tilde{\boldsymbol{C}}^{-1}\right]\nabla\Theta \end{aligned} \tag{20}$$

Here, we have the Piola heat flux vector $\boldsymbol{Q}$ derived from Duhamel's law (see Reference [2]), where k_{M} and k_{F} denotes the material conductivity coefficients for matrix and fiber roving. The time evolution of a prescribed boundary displacement is given by $\dot{\boldsymbol{q}}^{\mathrm{ref}}$ with the Lagrange multiplier $\boldsymbol{\lambda}_q$. The vector $\boldsymbol{g}$ denotes the gravitational force. The non-negative internal viscous dissipation D^{int} is given by

$$D^{\mathrm{int}} = \dot{\boldsymbol{C}}_v : \mathbb{V}(\boldsymbol{C}_v) : \dot{\boldsymbol{C}}_v \qquad \mathbb{V}(\boldsymbol{C}_v) = \frac{1}{4}\left(V_{\mathrm{vol}} - \frac{V_{\mathrm{dev}}}{n_{\mathrm{dim}}}\right)\boldsymbol{C}_v^{-1}\otimes\boldsymbol{C}_v^{-1} + \frac{V_{\mathrm{dev}}}{4}\mathbb{I}_{\mathrm{s}} : \boldsymbol{C}_v^{-1}\otimes\boldsymbol{C}_v^{-1}, \tag{21}$$

with the viscosity constants V_{vol} and V_{dev}, which represent the volumetric and deviatoric viscosity constants and the fourth-order symmetric projection tensor $\mathbb{I}_{\mathrm{s}}$. The operator $\otimes$ represents the standard dyadic product.

The total energy balance $\dot{\mathcal{H}}$ thus reads

$$\dot{\mathcal{H}} = \dot{T}(\dot{\boldsymbol{q}},\dot{\boldsymbol{v}},\dot{\boldsymbol{p}}) + \dot{\Pi}^{\mathrm{ext}}(\dot{\boldsymbol{q}},\boldsymbol{\lambda}_q,\dot{\boldsymbol{C}}_v,\tilde{\Theta},\dot{\Theta}) + \dot{\Pi}^{\mathrm{int}}(\dot{\boldsymbol{q}},\tilde{\Theta},\dot{\eta},\dot{\boldsymbol{C}}_v,\dot{\tilde{\boldsymbol{C}}},\dot{\tilde{J}},\dot{\tilde{\boldsymbol{C}}}_A,\boldsymbol{S},p,\boldsymbol{S}_A,\dots) \tag{22}$$

Note, that we define the superimposed fields ($\tilde{\boldsymbol{S}}$,$\tilde{p}$,$\tilde{\boldsymbol{S}}_A$,$\tilde{\boldsymbol{H}}$,$\tilde{\boldsymbol{B}}$), the viscous dissipation D^{int} as well as the Piola heat flux vector $\boldsymbol{Q}$ as parameters not as arguments. We obtain the total weak forms by variation with respect to the variables in the argument of Eqn. (22). With $\int_T \delta_*\dot{\mathcal{H}}\mathrm{d}t \equiv \int_T[\delta_*\dot{T} + \delta_*\dot{\Pi}^{\mathrm{ext}} + \delta_*\dot{\Pi}^{\mathrm{int}}]\mathrm{d}t = 0$, the weak forms which occur in both variants of the higher-order gradient formulation read

$$\int_T\int_{\mathcal{B}_0}\left[\frac{1}{\rho_0}\boldsymbol{p} - \dot{\boldsymbol{q}}\right]\cdot\delta\dot{\boldsymbol{v}}\mathrm{d}V\mathrm{d}t = 0 \qquad \int_T\int_{\partial\mathcal{B}_0}\left[-\boldsymbol{\lambda}_q\right]\cdot\delta\dot{\boldsymbol{q}}\mathrm{d}A\mathrm{d}t = 0$$

$$\int_T\int_{\mathcal{B}_0}\left[\eta + \frac{\partial\Psi}{\partial\Theta}\right]\delta\dot{\Theta}\mathrm{d}V\mathrm{d}t = 0 \qquad \int_T\int_{\mathcal{B}_0}\left[\frac{\mathrm{Div}[\boldsymbol{Q}]}{\Theta} + \frac{D^{\mathrm{int}}}{\Theta} + \dot{\eta}\right]\delta\tilde{\Theta}\mathrm{d}V\mathrm{d}t = 0$$

$$\int_T\int_{\mathcal{B}_0}\frac{1}{2}\left[\dot{\tilde{\boldsymbol{C}}} - \dot{\boldsymbol{C}}\right] : \delta\boldsymbol{S}\mathrm{d}V\mathrm{d}t = 0 \qquad \int_T\int_{\mathcal{B}_0}\left[\Theta - \tilde{\Theta}\right]\delta\dot{\eta}\mathrm{d}V\mathrm{d}t = 0$$

$$\int_T\int_{\mathcal{B}_0}\left[\frac{\partial\Psi}{\partial\boldsymbol{C}_v} + \dot{\boldsymbol{C}}_v : \mathbb{V}(\boldsymbol{C}_v)\right] : \delta\dot{\boldsymbol{C}}_v\mathrm{d}V\mathrm{d}t = 0 \qquad \int_T\int_{\partial\mathcal{B}_0}\left[\dot{\tilde{\boldsymbol{q}}} - \dot{\boldsymbol{q}}^{\mathrm{ref}}(t)\right]\cdot\delta\boldsymbol{\lambda}_q\mathrm{d}A\mathrm{d}t = 0$$

$$\int_T\int_{\mathcal{B}_0}\left[\dot{\tilde{J}} - \dot{J}\right]\delta p\mathrm{d}V\mathrm{d}t = 0 \qquad \int_T\int_{\mathcal{B}_0}\left[p - \left[\frac{\partial\Psi}{\partial\tilde{J}} + \tilde{p}\right]\right]\delta\dot{\tilde{J}}\mathrm{d}V\mathrm{d}t = 0$$

$$\int_T\int_{\mathcal{B}_0}\frac{1}{2}\left[\dot{\tilde{\boldsymbol{C}}}_A - \dot{\tilde{\boldsymbol{C}}}\right] : \delta\boldsymbol{S}_A\mathrm{d}V\mathrm{d}t = 0 \qquad \int_T\int_{\mathcal{B}_0}\left[\frac{1}{2}\boldsymbol{S}_A - \left[\frac{\partial\Psi}{\partial\tilde{\boldsymbol{C}}_A} + \tilde{\boldsymbol{S}}_A\right]\right] : \delta\dot{\tilde{\boldsymbol{C}}}_A\mathrm{d}V\mathrm{d}t = 0$$

$$\int_T\int_{\mathcal{B}_0}\left[\frac{1}{2}\boldsymbol{S} - \left(\frac{\partial\Psi}{\partial\tilde{\boldsymbol{C}}} + \frac{p}{2J(\tilde{\boldsymbol{C}})}\mathrm{cof}[\tilde{\boldsymbol{C}}] + \frac{1}{2}\boldsymbol{S}_A + \tilde{\boldsymbol{S}}\right)\right] : \delta\dot{\tilde{\boldsymbol{C}}}\mathrm{d}V\mathrm{d}t = 0$$

The weak forms associated with the higher-order gradient formulation in $\boldsymbol{F}$ (HF) are given by

$$\int_T\int_{\mathcal{B}_0}\left[\boldsymbol{S} : \frac{1}{2}\frac{\partial\dot{\boldsymbol{C}}}{\partial\dot{\boldsymbol{q}}} + \boldsymbol{P} : \frac{\partial\dot{\boldsymbol{F}}}{\partial\dot{\boldsymbol{q}}} - \dot{\boldsymbol{p}}\right]\cdot\delta_*\dot{\boldsymbol{q}}\mathrm{d}V\mathrm{d}t = 0 \qquad \int_T\int_{\mathcal{B}_0}\left[\dot{\tilde{\boldsymbol{F}}} - \dot{\boldsymbol{F}}\right] : \delta_*\boldsymbol{P}\mathrm{d}V\mathrm{d}t = 0$$

$$\int_T\int_{\mathcal{B}_0}\left[\boldsymbol{P} - \left(\boldsymbol{H} : \frac{\partial\boldsymbol{\Lambda}^{\mathrm{F}}}{\partial\dot{\tilde{\boldsymbol{F}}}} + \boldsymbol{B}\odot_3\frac{\partial\nabla\dot{\tilde{\boldsymbol{F}}}}{\partial\dot{\tilde{\boldsymbol{F}}}}\right)\right] : \delta_*\dot{\tilde{\boldsymbol{F}}}\mathrm{d}V\mathrm{d}t \qquad \int_T\int_{\mathcal{B}_0}\left[\nabla(\dot{\tilde{\boldsymbol{F}}}) - \dot{\tilde{\boldsymbol{\Gamma}}}\right]\odot_3\delta_*\boldsymbol{B}\mathrm{d}V\mathrm{d}t = 0$$

$$\int_T\int_{\mathcal{B}_0}\left[\boldsymbol{\Lambda}^{\mathrm{F}} - \tilde{\boldsymbol{\Lambda}}\right] : \delta_*\boldsymbol{H}\mathrm{d}V\mathrm{d}t = 0 \qquad \int_T\int_{\mathcal{B}_0}\left[\boldsymbol{H} - \left[\frac{\partial\Psi}{\partial\tilde{\Lambda}} + \tilde{\boldsymbol{H}}\right]\right] : \delta_*\dot{\tilde{\boldsymbol{\Lambda}}}\mathrm{d}V\mathrm{d}t = 0$$

$$\int_T\int_{\mathcal{B}_0}\left[\boldsymbol{B} - \boldsymbol{H} : \frac{\partial\boldsymbol{\Lambda}^{\mathrm{F}}}{\partial\dot{\tilde{\boldsymbol{\Gamma}}}}\right]\odot_3\delta_*\dot{\tilde{\boldsymbol{\Gamma}}}\mathrm{d}V\mathrm{d}t = 0$$

and the weak forms associated with the higher-order gradient formulation in $\boldsymbol{C}$ (HC) take the form

$$\int_T \int_{\mathcal{B}_0} \left[\boldsymbol{S} : \frac{1}{2}\frac{\partial \dot{\boldsymbol{C}}}{\partial \dot{\boldsymbol{q}}} + \boldsymbol{S}_G : \frac{1}{2}\frac{\partial \dot{\boldsymbol{C}}}{\partial \dot{\boldsymbol{q}}} - \dot{\boldsymbol{p}} \right] \cdot \delta_* \dot{\boldsymbol{q}} \mathrm{d}V \mathrm{d}t = 0 \qquad \int_T \int_{\mathcal{B}_0} \left[\dot{\tilde{\boldsymbol{C}}} - \dot{\tilde{\boldsymbol{C}}}_G \right] : \delta_* \boldsymbol{S}_G \mathrm{d}V \mathrm{d}t = 0$$

$$\int_T \int_{\mathcal{B}_0} \left[\frac{1}{2}\boldsymbol{S}_G - \boldsymbol{B} \odot_3 \frac{\partial \nabla \dot{\tilde{\boldsymbol{C}}}_G}{\partial \dot{\tilde{\boldsymbol{C}}}_G} \right] : \delta_* \dot{\tilde{\boldsymbol{C}}}_G \mathrm{d}V \mathrm{d}t \qquad \int_T \int_{\mathcal{B}_0} \left[\nabla(\dot{\tilde{\boldsymbol{C}}}_G) - \dot{\tilde{\boldsymbol{\Gamma}}} \right] \odot_3 \delta_* \boldsymbol{B} \mathrm{d}V \mathrm{d}t = 0$$

$$\int_T \int_{\mathcal{B}_0} \left[\boldsymbol{B} - \left[\frac{\partial \Psi}{\partial \tilde{\Gamma}} + \tilde{\boldsymbol{B}} \right] \right] \odot_3 \delta_* \dot{\tilde{\boldsymbol{\Gamma}}} \mathrm{d}V \mathrm{d}t = 0$$

The operator $\odot_3$ represents the triple construction of two tensors. Obviously, for the higher-order gradient formulation in $\boldsymbol{C}$, we have less weak forms and thus the tangent becomes substantially simpler.

In the next step, we discretize all quantities over the elements in space and time and transform the integrals to reference elements. For the shape functions in space, N, we use Lagrangian shape functions (see Reference [7]) and approximate the different mixed fields independently. Also we use the same shape functions for the Lagrangian multipliers as for their corresponding mixed fields. We use Lagrangian shape functions in time as well (see Reference [2]), given by

$$M_i(\alpha) = \prod_{\substack{j=1 \\ j \neq i}}^{k+1} \frac{\alpha - \alpha_j}{\alpha_i - \alpha_j}, \; 1 \leq i \leq k+1 \qquad \tilde{M}_i(\alpha) = \prod_{\substack{j=1 \\ j \neq i}}^{k} \frac{\alpha - \alpha_j}{\alpha_i - \alpha_j}, 1 \leq i \leq k \tag{23}$$

The time rate variables and mixed fields ($\boldsymbol{q}$,$\boldsymbol{v}$,$\boldsymbol{p}$,$\tilde{\Theta}$,Θ,η,$\boldsymbol{C}_v$,$\tilde{\boldsymbol{C}}$,$\tilde{\boldsymbol{C}}_A$,$\tilde{J}$,$\tilde{\boldsymbol{\Gamma}}$,$\tilde{\boldsymbol{\Lambda}}$,$\tilde{\boldsymbol{F}}$,$\tilde{\boldsymbol{C}}_G$) are approximated by

$$(\bullet)^{e,h} = \sum_{I=1}^{k+1} \sum_{A=1}^{n_{no}} M_I(\alpha) \mathrm{N}^A(\boldsymbol{\xi}) (\bullet)_I^{eA} \tag{24}$$

and the approximation of Lagrangian multipliers and variation fields ($\boldsymbol{\lambda}_q$,$\boldsymbol{S}$,$\boldsymbol{S}_A$,p,$\boldsymbol{B}$,$\boldsymbol{H}$,$\boldsymbol{P}$,$\boldsymbol{S}_G$,$\delta_* \bullet$) takes the form

$$(\bullet)^{e,h} = \sum_{I=1}^{k} \sum_{A=1}^{n_{no}} \tilde{M}_I \mathrm{N}^A (\bullet)_I^{eA} \tag{25}$$

Here, k is the polynomial degree in time and n_{no} is the number of nodes of the spatial discretization. We approximate each integral with the corresponding Gaussian quadrature rule and condense out the resulting formulation at the element level to a displacement and temperature formulation (see Reference [4]), after eliminating $\boldsymbol{p}$ and η. Note, all mixed fields, except $\boldsymbol{q}$ and Θ, are discontinuous at the boundaries of spatial elements. The internal variable $\boldsymbol{C}_v$ is solved on the element level using the Newton-Raphson method, not at each spatial quadrature point. Since the higher-order gradient formulation results in internal torques, the conservation of angular momentum must be corrected. For the procedure which is described in Reference [11], we obtain for the formulation in $\boldsymbol{F}$

$$\mathcal{J}_{n+1} - \mathcal{J}_n = \int_{t_n}^{t_n+1} \int_{\mathcal{B}_0} \left[\left(\boldsymbol{H} : \frac{\partial \boldsymbol{\Lambda}^{\mathrm{F}}}{\partial \dot{\tilde{\boldsymbol{F}}}} + \boldsymbol{B} \odot_3 \frac{\partial \nabla \dot{\tilde{\boldsymbol{F}}}}{\partial \dot{\tilde{\boldsymbol{F}}}} \right) \times \tilde{\boldsymbol{F}} \right] \mathrm{d}V \mathrm{d}t + \int_{t_n}^{t_n+1} \int_{\partial \mathcal{B}_0} [\boldsymbol{q} \times \boldsymbol{\lambda}_q] \mathrm{d}A \mathrm{d}t + \int_{t_n}^{t_n+1} \int_{\mathcal{B}_0} [\boldsymbol{q} \times \rho_0 \boldsymbol{g}] \mathrm{d}V \mathrm{d}t \tag{26}$$

and for the formulation in $\boldsymbol{C}$

$$\mathcal{J}_{n+1} - \mathcal{J}_n = \int_{t_n}^{t_n+1} \int_{\mathcal{B}_0} \left[\boldsymbol{B} \odot_3 \frac{\partial \nabla \dot{\tilde{\boldsymbol{C}}}_G}{\partial \dot{\tilde{\boldsymbol{C}}}_G} \times \tilde{\boldsymbol{F}} \right] \mathrm{d}V \mathrm{d}t + \int_{t_n}^{t_n+1} \int_{\partial \mathcal{B}_0} [\boldsymbol{q} \times \boldsymbol{\lambda}_q] \mathrm{d}A \mathrm{d}t + \int_{t_n}^{t_n+1} \int_{\mathcal{B}_0} [\boldsymbol{q} \times \rho_0 \boldsymbol{g}] \mathrm{d}V \mathrm{d}t \tag{27}$$

We use our In-House Matlab code fEMcon based on the implementation and ideas shown in Reference [7]. To solve the linear systems of equations we use the Pardiso solver from Reference [8]. For the assembly procedure of all n_{el} finite elements, we use the fast sparse routine shown in Reference [9].

3 NUMERICAL EXAMPLES

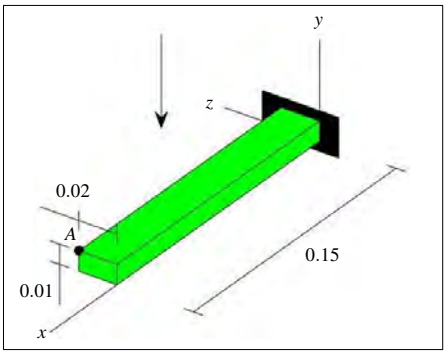

$\varepsilon_1 = 0.1e6$	$\beta_F = 1e-6$
$\varepsilon_2 = 100e6$	$c_F^0 = 200$
$k_M = 0.1$	$c_F^1 = 0.0002$
$\beta_M = 1e-6$	$\rho_0 = 1000$
$c_M^0 = 800$	$\Theta_\infty = 300$
$c_M^1 = 0.0008$	$T = 1$
$\varepsilon_3 = 0$	$TOL = 1e-4$
$k_F = 100$	$g = [0\ -2\ 0]$

Figure 1: Geometry, configuration and simulation parameters of the cantilever beam for $n_{el} = 24$.

As numerical example serves a simple cantilever beam which oscillates in a gravitational field. The geometry, configuration and simulation parameters can be found in Figure 1. The corresponding strain energy functions are

$$\Psi_M^{\text{iso}} = \frac{\varepsilon_1}{2}(\text{tr}[\boldsymbol{C}] - 3 - 2\ln(J)) \quad \Psi_M^{\text{vol}} = \frac{\varepsilon_2}{2}\left(\ln(J)^2 + (J-1)^2\right)$$
$$\Psi_X^{\text{cap}} = c_X^0(1 - \Theta_\infty c_X^1)(\Theta - \Theta_\infty - \Theta\ln\frac{\Theta}{\Theta_\infty}) - \frac{1}{2}c_X^0 c_X^1(\Theta - \Theta_\infty)^2$$
$$\Psi_F^{\text{ela}} = \frac{\varepsilon_3}{2}(\text{tr}[\boldsymbol{CM}] - 1)^2 \quad \Psi_{\text{HOG}}^{\text{X}} = l^2\left(I_6^{\text{X}}\right)^2$$

The elastic part of the fiber roving Ψ_F^{ela} can be found in [10] and for the capacitive part the function Ψ_X^{cap} in Reference [2] . We use a quadratic serendipity mesh (20 nodes) with $n_{el} = 24$ and approximate $\tilde{J}$ linear and $\tilde{\boldsymbol{C}}_A$ constant to avoid potential locking effect. We introduce a length scale parameter l^2 with $c = \varepsilon_1 l^2$ for the material parameters of $\Psi_{\text{HOG}}^{\text{X}}$. Futhermore, the strain energy function of the viscous matrix part is given by $\Psi_M^{\text{vis}} = \Psi_M^{\text{iso}}(\boldsymbol{C}\boldsymbol{C}_v^{-1}) + \Psi_M^{\text{vol}}(\boldsymbol{C}\boldsymbol{C}_v^{-1})$.

First, we compare the stiffening behavior of the different higher-order gradient fomulations. In Figure 2 we can see that both formulations stiffen the bending behavior of the beam (HF and HC). However, it can also be done by the $\nabla\boldsymbol{C}$ formulation, although not to the same level (green). By adjusting the material parameters, we obtain a similar behavior here, too (blue). When we look at the angular momentum in Figure 3, we can see it is perfectly preserved for the different formulations. This also shows that the correction of the internal moments as a result of the gradient formulations. In Figure 4 we can see the increasing temperature by the viscous dissipation. As expected, the major

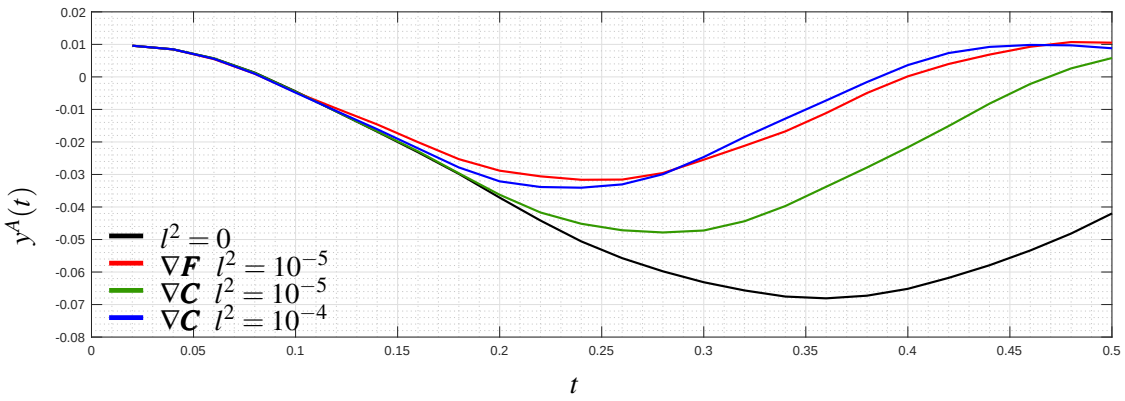

Figure 2: Trajectory of point A for the parameters shown in Figure 1 and the different formulations and $(\boldsymbol{a}_0)^T = [1\ 0\ 0]$.

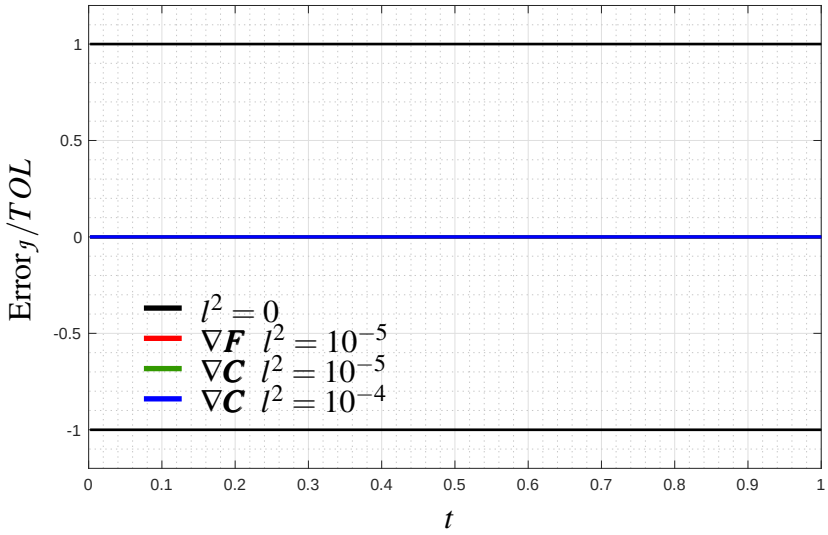

Figure 3: Error of angular momentum $\mathcal{J}$ for the parameters shown in Figure 1 and the different formulations and $(\boldsymbol{a}_0)^T = [1\ 0\ 0]$.

increase in temperature is found at the mounting where the largest deformations occur. Next we check the objectivity of the new superimposed fields of the higher-order gradient formulation on the basis of a free-flying beam. Therefore, we set the initial rotational speed to $\boldsymbol{\omega}^T = [2\pi\ 2\pi\ 2\pi]$ and simulate until $T = 10$. In Figure 6-10 we can see that each higher-order gradient formulation and length scale parameter conserve the total energy. For the high l^2, a slightly higher energy error is observed, but this is also within the tolerance. For example, this can be explained by the fact that although the higher stiffness, we keep the time step size constant. In Figure 5 we show the current configuration and v. Mises equivalent stress σ_{VM} for $t = 10$. As expected, the beam is deformed by the rotation and shows the larger stresses at larger deformations.

4 CONCLUSIONS

We have shown that it is possible to formulate a higher-order gradient material formulation in terms of the right Cauchy-Green tensor. This is a remarkable result, because this formulation requires considerably less numerical effort and we can formulate the superimposed field directly in terms of $\nabla \boldsymbol{C}$ and thus achieve a roving direction independence. Also, both formulations work in a thermo-visoelastic context. And we have also shown that the higher-order energy-momentum time integrators

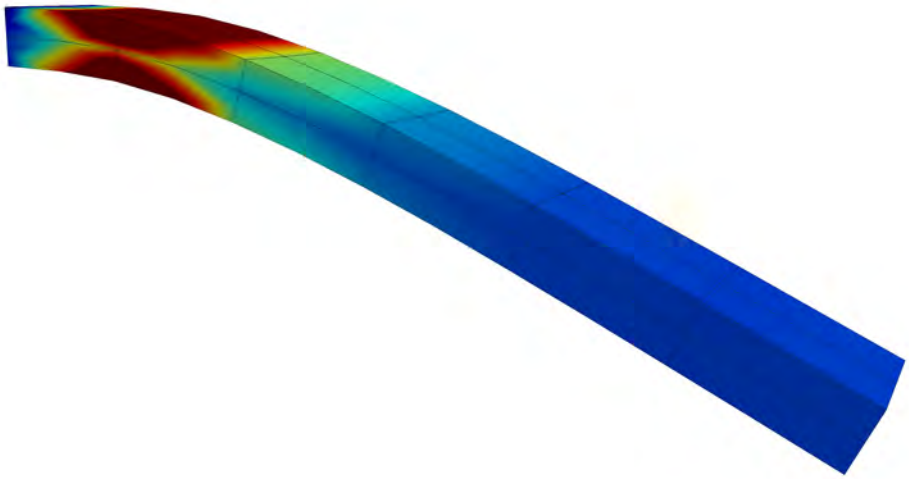

Figure 4: Configuration and temperature distribution Θ for the parameters shown in Figure 1, $(\boldsymbol{a}_0)^T = [1\ 0\ 0]$, $t = 0.24$, $\nabla \boldsymbol{C}$ and $l^2 = 10^{-4}$.

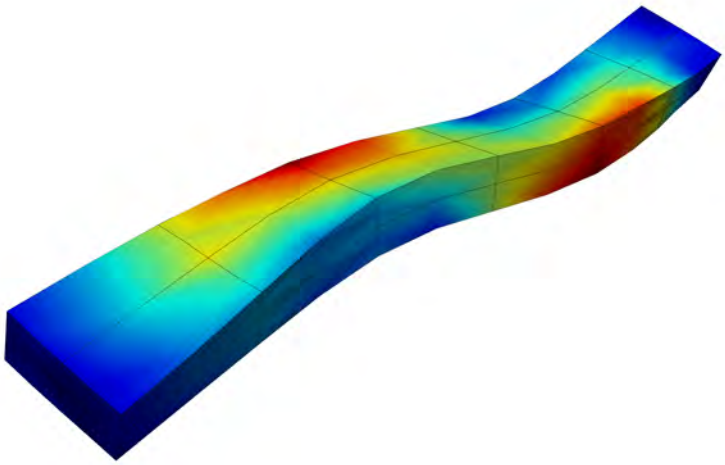

Figure 5: Configuration and v. Mises equivalent stress σ_{VM} for the parameters shown in Figure 1, $(\boldsymbol{a}_0)^T = [1\ 0\ 0]$, $\boldsymbol{\omega}^T = [2\pi\ 2\pi\ 2\pi]$, $t = 10$, $\nabla \boldsymbol{C}$ and $l^2 = 10^{-4}$.

conserve energy in all cases. In the next step, we want to investigate other material formulation and will look on potential locking effects.

Acknowledgments

The authors thank the 'Deutsche Forschungsgemeinschaft (DFG)' for the financial support of this work under the grant GR3297/4-2 and GR3297/6-1 as well as Matthias Bartelt (GR 3297/2-2) for providing the programming basis for the current implementation.

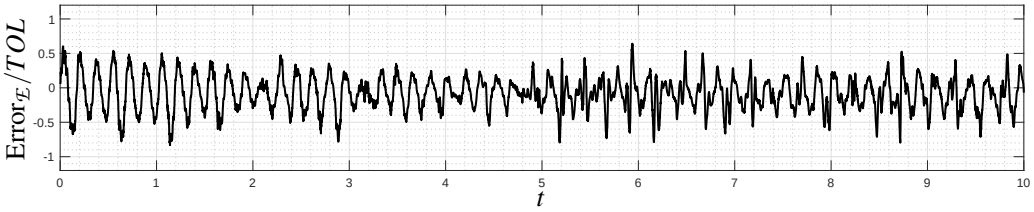

Figure 6: Error of energy $\mathcal{E}$ for the parameters shown in Figure 1, $(\boldsymbol{a}_0)^T = [1\ 0\ 0]$, $\boldsymbol{\omega}^T = [2\pi\ 2\pi\ 2\pi]$, $T = 10$ and $l^2 = 0$.

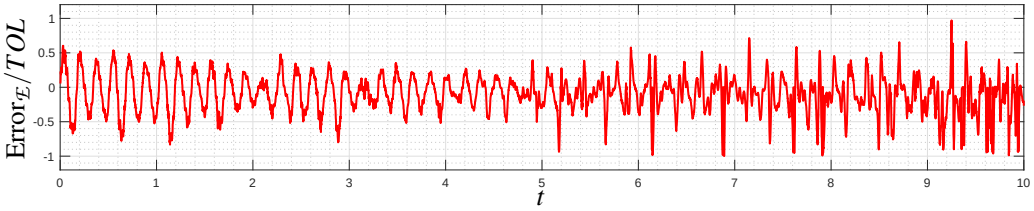

Figure 7: Error of energy $\mathcal{E}$ for the parameters shown in Figure 1, $(\boldsymbol{a}_0)^T = [1\ 0\ 0]$, $\boldsymbol{\omega}^T = [2\pi\ 2\pi\ 2\pi]$, $T = 10$, $\nabla \boldsymbol{F}$ (HF) and $l^2 = 10^{-5}$.

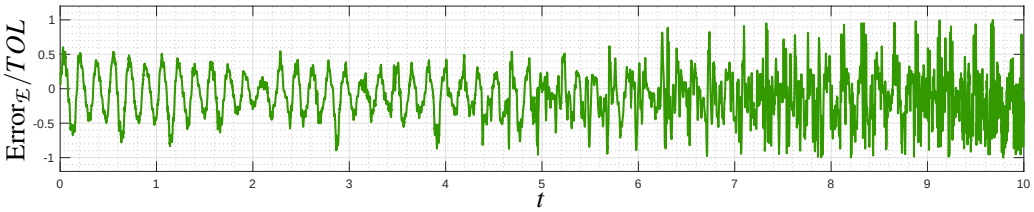

Figure 8: Error of energy $\mathcal{E}$ for the parameters shown in Figure 1, $(\boldsymbol{a}_0)^T = [1\ 0\ 0]$, $\boldsymbol{\omega}^T = [2\pi\ 2\pi\ 2\pi]$, $T = 10$, $\nabla \boldsymbol{F}$ (HF) and $l^2 = 10^{-4}$.

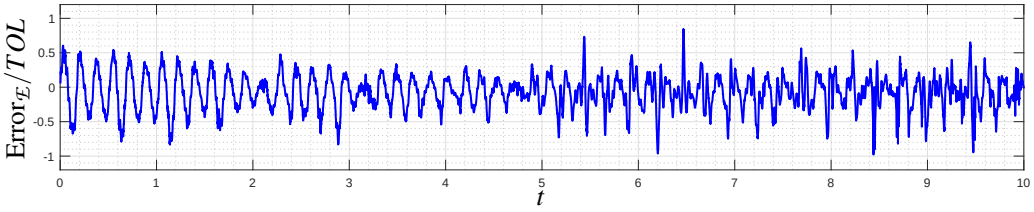

Figure 9: Error of energy $\mathcal{E}$ for the parameters shown in Figure 1, $(\boldsymbol{a}_0)^T = [1\ 0\ 0]$, $\boldsymbol{\omega}^T = [2\pi\ 2\pi\ 2\pi]$, $T = 10$, $\nabla \boldsymbol{C}$ (HC) and $l^2 = 10^{-4}$.

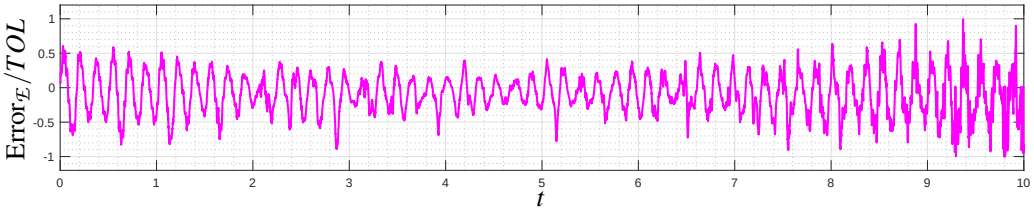

Figure 10: Error of energy $\mathcal{E}$ for the parameters shown in Figure 1, $(\boldsymbol{a}_0)^T = [1\ 0\ 0]$, $\boldsymbol{\omega}^T = [2\pi\ 2\pi\ 2\pi]$, $T = 10$, $\nabla \boldsymbol{C}$ (HC) and $l^2 = 10^{-3}$.

REFERENCES

[1] Asmanoglo, T., Menzel., A. (2017) A multi-field finite element approach for the modelling of fibre-reinforced composites with fibre-bending stiffness. *Comput. Methods Appl. Mech. Engrg.*, 317:1037–1067.

[2] Groß, M., Dietzsch, J., and Bartelt, M. (2018). Variational-based higher-order accurate energy–momentum schemes for thermo-viscoelastic fiber-reinforced continua. *Comput. Methods Appl. Mech. Engrg.*, 336, 353–418. https://doi.org/10.1016/j.cma.2018.03.019

[3] Simo, J. C., Taylor, R. L., and Pister, K. S. (1985). Variational and projection methods for the volume constraint in finite deformation elasto-plasticity. *Comput. Methods Appl. Mech. Engrg.*, 51(1–3), 177–208. https://doi.org/10.1016/0045-7825(85)90033-7

[4] Schröder, J., Viebahn, V., Wriggers, and P., Balzani, D. (2016). A novel mixed finite element for finite anisotropic elasticity; the SKA-element Simplified Kinematics for Anisotropy. *Comput. Methods Appl. Mech. Engrg.*, 310:475–494.

[5] J. Dietzsch and M. Groß, Mixed Finite Element Formulations for Polyconvex Anisotropic Material Formulations in WCCM-ECCOMAS2020.

[6] Ferretti, M., Madeo, A., dell'Isola, F., & Boisse, P. (2014). Modeling the onset of shear boundary layers in fibrous composite reinforcements by second-gradient theory. Zeitschrift Fur Angewandte Mathematik und Physik, 65(3), 587–612.

[7] Bartelt, M., Dietzsch, J., and Groß, M. (2018). Efficient implementation of energy conservation for higher order finite elements with variational integrators. *Math. Comput. Simulat.*, 150, 83–121. https://doi.org/10.1016/j.matcom.2018.03.002

[8] Alappat, C., Basermann, A., Bishop, A. R., Fehske, H., Hager, G., Schenk, O., Thies, J., and Wellein, G. (2020). A Recursive Algebraic Coloring Technique for Hardware-efficient Symmetric Sparse Matrix-vector Multiplication. *ACM Transactions on Parallel Computing*, 7(3). https://doi.org/10.1145/3399732

[9] Engblom, S., and Lukarski, D. (2016). Fast Matlab compatible sparse assembly on multicore computers. *Parallel Computing*, 56, 1–17. https://doi.org/10.1016/j.parco.2016.04.001

[10] Dal, H., Gültekin, O., Aksu Denli, F., and Holzapfel, G. A. (2017). Phase-Field Models for the Failure of Anisotropic Continua. *PAMM*, 17(1). https://doi.org/10.1002/pamm.201710027

[11] Groß, M., Dietzsch, J., and Röbiger, C. (2020). Non-isothermal energy–momentum time integrations with drilling degrees of freedom of composites with viscoelastic fiber bundles and curvature–twist stiffness. Computer Methods in Applied Mechanics and Engineering, 365, 112973. https://doi.org/10.1016/j.cma.2020.112973